The Sun as an X–ray Star. II: Using the Yohkoh/SXT-derived Solar Emission Measure vs. Temperature to Interpret Stellar X-ray Observations

G. Peres[1], S. Orlando[2] and F. Reale

Dipartimento di Scienze Fisiche ed Astronomiche, Sezione di Astronomia, Piazza del Parlamento 1, 90134 Palermo, Italy

R. Rosner

Dept. of Astronomy and Astrophysics, University of Chicago; Enrico Fermi Institute, Chicago, Illinois, USA

H. Hudson

Solar Physics Research Corp., 4720 Calle Desecada,
Tucson, Arizona 85718, USA

ABSTRACT

This paper is the second of a project dedicated to use solar Yohkoh/SXT data as a guide and a template to interpret data on stellar coronae.

In the light of the large difference in scope and approach between solar and stellar studies we have developed a method to translate Yohkoh/SXT data of the whole solar corona into stellar-like data, i.e. to put them in the same format and context as the stellar ones. First from the Yohkoh/SXT images we derive the whole–Sun X-ray emission measure vs. temperature (EM(T)), in the range $10^{5.5}$ K -10^{8} K, during the specific observation. Then, we synthesize the solar X-ray spectrum; finally, we fold the spectrum through the instrumental response of non-solar X-ray observatories, for instance Rosat/PSPC and ASCA/SIS. Finally, we analyze such solar coronal data in the same band and with the same methods used for stellar observations allowing a direct and homogeneous comparison with them.

In this paper we present in detail our method and, as an example of results, we show and discuss EM(T) and stellar-like spectra for three phases of the solar cycle: maximum, intermediate phase, and minimum. The total amount and the distribution of the emission measure change dramatically during the cycle, in particular at temperatures above 10^6 K. We also show the EM(T) of the whole solar corona during a large flare.

The Rosat/PSPC- and ASCA/SIS-like X-ray spectra of the Sun as a star that we obtain are discussed in the context of stellar coronal physics.

---

[1]e-mail: peres@oapa.astropa.unipa.it

[2]Solar System Division – ESA Space Science Dept., ESTEC, Postbus 299, NL–2200 AG Noordwijk, The Netherlands

The Sun's coronal total luminosity in the Rosat/PSPC band ranges from $\approx 2.7 \times 10^{26}$ erg s^{-1} (at minimum) to $\approx 4.7 \times 10^{27}$ erg s^{-1} (at maximum).

We discuss future developments and possible applications of our method.

Subject headings: coronae: Sun, stars, X-ray observations

1. Introduction

It is customary to assume that soft X-ray observations of coronae on late–type stars (for which one has no imaging information) can be interpreted in the context of the "solar–stellar analogy": the presumption is that the coronae of these stars are the result of physical processes that are similar — if not identical — to those leading to the solar corona (cf. Rosner, Golub, & Vaiana 1985). One obvious question is whether this assumption is correct and, further, how one would go about testing it.

One key test is to determine whether the distribution of plasma temperatures in stellar coronae resembles that of the solar corona. To date, most of the focus of temperature studies for stellar coronae has been on so–called "one–" or "two–temperature" component analyses, based on imaging proportional counter data from either the *Einstein*, Rosat (Roentgen Satellit) or ASCA (Advanced Satellite for Cosmology and Astrophysics) observatories (e.g. Schmitt et al. 1990, Guedel et al. 1997). On the other hand, studies of the temperature distribution of the solar coronal plasma have focused on the temperature distribution within geometrically well–defined (loop or other) structures (Rosner, Tucker and Vaiana, 1978; Serio et al., 1981).

There is a substantial literature on the question of the temperature distributions of coronal plasmas (Pottasch 1965, Withbroe 1975, Craig and Brown 1976). As early as 1978, Pye et al. pointed out that the differential emission measure, $DEM(T)$, defined in the simplest case by

$$f \sim \int d^3r \; n_e^2(T) P(T) = \int dx \; dy \quad \int dT \; DEM(T) \; P(T) \quad \text{ergs s}^{-1} \, , \tag{1}$$

(where f is the flux observed at Earth, $\int dx \; dy$ is an integration in the plane of the sky, and $\int \; dT$ is the integration in temperature along the line-of-sight), is quite broad even in quiescent regions, well away from obvious active regions and transient (flaring) loop structures. It is commonly stated that "typical" coronal temperatures for the Sun are in the range $2 - 3 \times 10^6$ K for the quiescent corona, and $\sim 10^7$ K for flaring structures (see, e.g., Withbroe & Noyes 1977), i.e., that the coronal plasma distribution is fundamentally bimodal in temperature. More recently Schmelz et al. (1997) have studied the DEM for active regions using SMM/XRP and Yohkoh/SXT, and Bornmann and Matheson (1990) have derived the temperatures of active regions.

Also studies of the emission measure distributions for late–type stars (viz., Schmitt et al. 1990) suggest a bi-modal temperature structure, peaking at $\sim 2 \times 10^6$ K and $\sim 1 - 2 \times 10^7$ K.

The key question is then: can one reconcile the stellar observations with what is seen on the Sun? This point is rather crucial, because essentially all X-ray observations of late–type stars have been premised on the idea that the Sun is in fact an appropriate model for the coronae on these other stars (cf. Rosner, Golub, & Vaiana 1985).

A direct comparison of the Sun to other stars is not easy, because the scope and the methods of solar coronal observations have been traditionally different from those of the stellar ones. The former often concentrate on the detailed analysis of particular phenomena or structures, and only limited attention is dedicated to the global emission of the solar corona; stellar observations, instead, necessarily observe a star as a whole. The observing instruments themselves are very different: the spectral diagnostic work on stellar coronae has been mostly carried out with imaging proportional counters or charge coupled devices (CCDs) used in photon counting mode and, therefore, with moderate spectral resolution; the spectroscopic X-ray solar observations instead have used Bragg crystals with extremely high resolution (but mostly around He-like ions line complexes), and imaging solar observations in soft X-rays have used filter ratio methods first developed during the Orbiting Solar Observatories and *Skylab* eras (Vaiana, Krieger and Timothy, 1973; Vaiana et al. 1974). While comparisons between the solar and the stellar coronae have been easily made in general and coarse terms, direct and accurate comparisons have not been possible, because solar and stellar observations typically have very different signal–to–noise ratio and kind of physical information. A possible solution which we use here is to put solar and stellar observations in a similar format and context, so as to allow a direct comparison.

Our approach is based on direct experimental measurements made with the Soft X-ray Telescope (SXT) on board Yohkoh. The Yohkoh satellite has brought a breakthrough in solar physics: launched at the end of August 1991, at the maximum of solar activity, it has provided a continuous sequence of daily full–disk X-ray images of the Sun, complemented by a wealth of more specialized observations since the launch, through the solar minimum and even now during the ascending phase of the new cycle; it has observed a large variety of phenomena and events and has followed the long– and short–term evolution of the corona. In particular Yohkoh/SXT, the imaging X-ray telescope, has collected a very large number of images of the whole disk with angular (5" or 10" pixel size) and time resolution adequate to follow many of the events occurring in the solar corona.

The essence of our method is to translate the solar Yohkoh/SXT data into a format virtually identical to that of stellar observations made with an X-ray instrument, for instance the non-solar Rosat/PSPC (Position Sensitive Proportional Counter) or ASCA/SIS (Solid-state Imaging Spectrometer), apply to them standard methods of stellar analysis, and compare the results with those of stellar X-ray studies.

We first derive the distribution of emission measure vs. temperature of the whole corona, EM(T), from the Yohkoh images. Then, from the EM(T), by means of a spectral synthesis code and the known spectral response of non-solar X-ray observatories, we synthesize stellar–like observations of the Sun, as if located at stellar distances.

Each phase of the analysis produces a result of interest by itself: first, the distribution of the emission measure vs. temperature – EM(T) – of the whole solar corona (see Orlando et al. 1999a, henceforth Paper I); second, the relevant X-ray spectrum, both at the telescope entrance and folded through the instrument of interest, and, third, the spectral analysis of the solar corona in a stellar-like format. Each of them is important in the study of the Sun as a star. Our findings should allow us to test several of the fundamental tenets of the "solar–stellar connection" argument, including assumptions regarding the overall solar coronal temperature structure and the level of total flux and temperature variability as a function of activity level, as discussed in section 4 below.

A fundamental quality of Yohkoh/SXT observations is to provide the spatial distribution and location of the solar plasma at various temperatures: we can in principle identify and evaluate the contribution of specific structures and events both to the EM(T) and to the whole solar X-ray spectrum. Similar characteristics in stellar X-ray spectra may then indicate the presence of similar structures on the other stars.

Since stellar data collected by Rosat/PSPC and ASCA/SIS are moderate resolution spectra, they are not directly comparable with the photometric wide-band data of Yohkoh/SXT or of any other X-ray broad-band instrument such as the X–ray Sensors (XRS) on board the Geosynchronous Operational Environmental Satellite (GOES) (Hanser and Sellers 1996, Bornmann et al. 1996). The fact that the spectral bandpasses of solar instruments are usually very different from those on non-solar ones makes it more difficult to compare the relevant solar data to stellar observations. Indeed for a careful synthesis of the Sun's luminosity values and spectra folded with the Rosat/PSPC and ASCA/SIS instrumental response we need to derive the solar X-ray spectrum. In this respect a key point of our method is to derive the solar X-ray spectrum from the distribution of emission measure vs. temperature obtained from the many pixels in Yohkoh/SXT multiband data. A solar instrument with high spectral resolution and coverage, accompanied by adequate angular resolution and full–disk imaging, would be even more appropriate for our task, but such an instrument is presently not available.

Our paper is structured as follows: We describe the steps of our method in section 2 and discuss the relevant results at various phases of the Sun's activity cycle in section 3. In section 4 we discuss our findings and in section 5 we draw our conclusions and sketch some additional aspects of our project.

2. The method

In Fig. 1 we present the general scheme of our method in the various steps which we discuss in the following.

2.1. Deriving the Whole Sun Emission Measure Distribution vs. Temperature

The first step is to generate the EM(T) of the whole corona from full–disk images taken with Yohkoh/SXT.

The standard Yohkoh data analysis (Tsuneta et al. 1991; Morrison 1994) yields the value of T and of EM in any imaged pixel from the ratio of fluxes measured in two images (typically taken within a few minutes during typical full–disk observations and seconds during flare mode), in two different bands - i.e. through two different filters. It is customarily assumed isothermal plasma within each pixel, whose size is either 5" $\times$ 5", in full–disk images, or 2".5 $\times$ 2".5 in partial frame observations.

For the non-flaring Sun we have selected sequences of full–disk observations made through the Al 1265 Å filter (in the following Al.1), and the filter made by a sandwich of Al 2930 Å, Mg 2070 Å, Mn 562 Å, C 190 Å (AlMg). Such a combination is very often adopted for full–disk observations outside flares since it allows to measure temperatures in the 10^6 K -10^7 K range, typical of the non–flaring corona; in this temperature range the flux ratio AlMg/Al.1 varies from 0.2 to 0.7.

The usual filter selection for flares is, instead, the couple Be 119 μm (Be119) and Al 11.4 μm (Al12). Section 2.2 discusses more in detail flare observations and the slightly modified method we use for them. The flux ratio of the Be119/(2 $\times$ Al12) bands ranges from 0.4 to 2 for T ranging from 4×10^6 K to 2×10^7 K.

The standard determination of T and EM is based on the spectral model of Mewe, Gronenschild and van den Oord (1985), assuming ionization equilibrium. We have used its most updated version (Mewe, Lemen, and van den Oord 1986; Kaastra, J.S. 1992; Mewe, Kaastra and Liedahl, 1995 and references therein) the so called MEKAL spectral model, one of the most complete spectral models, in view of its wide use in the astrophysical community. We have consistently used this model in every step of our analysis, from the determination of the filter response and of the filter ratio vs. plasma temperature, to the final step, namely the spectral fitting of the synthesized stellar–like data.

The brightness distribution of the solar corona ranges over several orders of magnitude, from coronal holes to flares, and certainly over a dynamic range much larger than that of the CCD in the focal plane of SXT. In order to cover, nevertheless, such a large dynamic range, the observing sequences typically include several exposures with integration times differing by large factors (e.g. 78 ms and 2668 ms for the Al.1 sequence of January 6 1992, see Table 1). It may easily happen that, in such sequences, a long exposure detects well the faint coronal regions but is saturated in the brighter regions and, viceversa, that the short exposures detect well the bright regions and poorly the faint ones. Therefore, whenever needed, we take advantage of the whole observing sequence to build a complete description of the emission measure vs. temperature: we exclude the overexposed regions from the long exposure image and take them, instead, from an image of the same sequence with an exposure time short enough to grant good data and analysis in that region. Such a feat is quite straightforward within the Yohkoh standard data analysis system.

From the pixel map of temperature and the emission measure, we derive the *global distribution of emission measure vs. temperature*: we first divide the temperature range into bins and then sum the emission measure of all the pixels which belong to the same temperature bin.

The emission measure distribution provides, by itself, important insight into coronal physics; for instance it shows the relative role of solar coronal plasma at different temperatures in determining the X-ray emission (cf. also Watanabe et al., 1995).

Note that the EM(T) we compute is different from the DEM(T) mentioned in Section 1 because it is the line-of-sight averaged emission measure distributed across the solar corona, and it is different also from the temperature distribution of emission measure within a single pixel's line of sight.

2.1.1. Screening of pixels

A plain application of the above method to all the pixels of a Yohkoh/SXT image may easily lead to very large errors in the final EM(T) distribution. Below 10^6 K they can amount to more than one order of magnitude (see Paper I). A screening criterion allows us to avoid these errors. The crucial aspect is that each Sun image alone does not have an appropriate signal–to–noise ratio over the whole corona, but only over parts of it. Most of the full–disk observations are designed to alleviate this problem through observations made in rapid sequence and of increasing exposure time. However the typical choice, probably dictated by the need to follow rapidly evolving phenomena, of only two exposure times which typically differ by a factor of a few hundreds does not solve the problem entirely. Some pixels of intermediate brightness may have, therefore, in one (or all) of the images a rather low number of photons, thus leading to a large statistical error, which gives a large error in the filter ratio and, ultimately, in the temperature and emission measure values.

When this error occurs in the low temperature part of the instrument response, i.e. at 2 MK or less, the very steep instrumental response vs. T leads to a still larger error in the emission measure determination (Tsuneta et al. 1991; Paper I).

In Paper I, we have found that the application of the method to all the pixels without a screening criterion based on the signal–to–noise ratio easily leads to an EM monotonically decreasing from $10^{5.5}$ K to 10^8 K (cf. Fig. 12 in Paper I). In particular the emission measure values below 10^6 K are too large by orders of magnitude (up to three orders of magnitude at $T = 10^{5.5}$ K, cf. Paper I). One instead expects that the EM(T) monotonically increases for $T < 10^6$ K and reaches a maximum around 10^6 K, as invariably shown by many measurements optimized for that temperature range (for a recent example cf. Brosius et al., 1996).

In order to devise an accurate criterion to discard the low signal–to–noise pixels, at the same time retaining crucial information on the low temperature (or faint) corona, we have made an extensive set of simulations of the overall system performance at various photon count levels and various temperatures (Paper I) so as to select the appropriate minimum number of photon counts per pixel, as the appropriate threshold for inclusion in our analysis. We adopt the standard SXT gain factor of 100 electrons per Data Number (in the following DN) for this purpose, which yields ≈ 0.5 photons per DN at 2 MK (in both filters). The resulting pixel selection procedure, presented in more detail in the companion Paper I, can be sketched as follows:

- Within a sequence with, at least, observations in two filters and two exposure times for a total of, at least, four images, we select from the longest exposure images (see Table 1 for typical examples) only those pixels with more than 10 photons and which are not saturated.
- The pixels excluded because overexposed are taken from the image of the same sequence with a shorter exposure time.
- If there are still overexposed areas in the composite exposures data, the procedure is repeated on still shorter exposures (if available) until all the image is covered.

In any case, if some pixels not properly exposed (i.e. which collected less than 10 photons) still remain at the end of this phase of the analysis, they are discarded.

It is worth noting that this procedure leads naturally to a distribution for $T < 10^6$ K in remarkable agreement with the results of EUV measurements (Brosius et al., 1996; Landi and Landini, 1997)[3].

As mentioned above, this method works at its best if the observing sequence contains a series of images with different exposure times, adequately sampling the large dynamic range of the Sun's X-ray brightness.

The implicit assumption is that the coronal EM(T) does not change appreciably within the few minutes covered by the observing sequence of images. We have tested that this assumption is practically always correct with the exception of flares which, however, we handle with a different procedure, discussed below.

More details on the method and on the relevant simulations are discussed in Paper I.

[3]In order to improve the signal–to–noise ratio, we *may* also first integrate any image over 2×2 pixels and average over the five possible positions of the integration mask: i.e. centered as well as shifted by one pixel in the north, south, east and west direction, so as to avoid any bias caused by the specific integration mask. The results presented in the following, however, are not derived with such an optional spatial integration.

2.1.2. Binning of the temperature range

For the determination of the EM(T), we have chosen a temperature binning uniform in log T as the best compromise among several alternatives:

- a spacing uniform in T yields either an oversampling at high T or an undersampling at low T;
- a spacing proportional to dT/dr (where r is the value of the ratio of filtered flux in the specific Yohkoh/SXT bands used) is adequate for the temperature discrimination with the specific filter ratio but may not be appropriate when using simultaneously several filter ratios to build a complete EM(T) of the Sun (see "Flares", below); also it would be difficult to compare the EM contribution of each temperature bin to the total, given the non uniform size of bins over which the EM summing is made;
- a uniform $\Delta logT$ spacing yields an adequate discrimination of temperature, even when different filter ratios are simultaneously used, it allows a straightforward evaluation of the EM contribution at various T, and a straightforward comparison with typical radiative losses or filter ratio curves, which are better presented vs. log T.

2.2. Flares

Flares are the most evident, dynamic and luminous tracers of solar and stellar coronal activity. They are characterized by coronal plasma temperature at $\sim 10^7$ K and by a large emission measure, typically comparable to that of the entire non-flaring corona. The method described in the previous sub–section can also be used to derive the EM(T) of the whole solar corona during flares, as long as proper care is given for the different procedure for collecting flare data, namely the SXT flare mode.

An X-ray flare typically does not involve the whole solar corona, and is fundamentally related to the active region, site of the flare itself. It is also relatively independent of what occurs in parts of the corona far away. During flares (Ogawara et al. 1991, Tsuneta et al. 1991), Yohkoh/SXT takes images only of a small area including the flaring region as fast sequences of "partial frames", consisting of 64×64 pixels of 2.5" $\times$ 2.5" size; several filters are normally used including the Be119 and the Al12 filters. Obtaining the EM of the whole corona during a flare, therefore, requires deriving separately the EM of the non-flaring Sun and that of the flare, and finally adding the two.

Since the flare is largely independent of the remaining Sun, we can derive the EM(T) of a background Sun and a flare occurring at different times; in this way we can achieve a larger set of combinations of flares and non-flaring background corona, with the possibility to simulate a larger set of different configurations to be compared with stellar observations.

2.3. Generating the stellar-like spectrum

From the emission measure vs. temperature we derive the emitted spectrum of the corona with the MEKAL spectral code and then fold it through the instrumental response of the stellar instrument of interest. In the following we will fold the spectra with the response of Rosat/PSPC and of ASCA/SIS since they are among the X-ray observatories most used for stellar coronae observations. In order to generate a realistic stellar–like spectral observation of the Sun we assume plausible values for the star's distance, for the exposure time, and for the number of collected photons.

Equation (2) yields the photon counts in each channel of the simulated spectrum:

$$C_j = \frac{t}{4\pi d^2} \int dE \, \frac{A(E)\ M(j,E)}{E} \quad \sum_k P(T_k,E)\ EM(T_k) \tag{2}$$

where C_j is the number of counts in the j-th spectral channel of the detector, t is the observing time, d is the distance of the "star", E is the energy of the photons, *A(E)* the effective area of the instrument vs. photon energy, including the spectral response of the telescope, of the filters and of the detector, *M(j,E)* is the detector response matrix (i.e. the probability that a photon of energy E is detected in the j-th energy channel), EM(T_k), the emission measure in the k-th temperature bin derived from the Yohkoh/SXT images, $P(T_k,E)$ the spectrum emitted by an optically thin isothermal plasma with the appropriate elemental abundances. The sum over the temperature bins provides the global spectrum of the solar plasma and the integral over energy takes into account also the instrumental response.

In order to obtain a realistic simulation of stellar X-ray observations, we randomize the photon counts in each energy channel of the specific instrument (e.g. Rosat/PSPC or ASCA/SIS) of the synthesized stellar spectrum according to Poisson statistics. The Poisson randomization is performed using the rejection method applied to the Poisson distribution (Press et al. 1986).

In our rendering of the Sun as a star, we have generated spectra with a total number of photons typical of good stellar observations, namely a few thousand photons with Rosat/PSPC, and a few ten thousand photons with ASCA/SIS. Of course we can simulate much higher numbers of collected photons but we want to compare our results with stellar observations also at comparable signal–to–noise level.

Both ROSAT/PSPC- and ASCA/SIS-simulated spectra are computed, according to Eq. (2), within the Analysis System for Astrophysical Plasmas (ASAP) described by Maggio et al. (1994). ASAP includes all the spectral synthesis routines we need and can compute any folded spectrum, as long as the spectral characteristics and the relevant instrumental response are available.

The synthesized photon count spectrum is put in a format identical to that of real non-solar observations and can therefore be subject to the standard data analysis system used for the specific non-solar instrument of interest.

In the following section we will show examples of such synthesized spectra.

3. Results

3.1. The Yohkoh data

Given the almost continuous monitoring of the Sun made by Yohkoh/SXT, started in August 1991, a large wealth of solar coronal data is available. They cover the Sun evolution over time scales ranging from seconds to years and give crucial information on a wide variety of structures and events. Here we present a few representative cases to illustrate our method and to show a few sample results, namely the Sun at three phases of the solar cycle: close to the maximum, in an intermediate phase, and at the minimum. In particular, we have selected an observing sequence on 6 Jan 92, around 21:40 UT, another one on 27 Jul 93 around 11:28 UT, and a third one on 1 Jun 94 around 6:35 UT, respectively.

Fig. 2 shows the composite images from multiple exposures used in our analysis. It is worth noting that when choosing the minimum of solar activity, particular care was taken to select a phase showing very little, if any, sign of activity.

We have also studied the Sun during a few flares of different duration and intensity; we consider here a very intense, Long Duration Event (LDE) that occurred on 2 November 1992 and lasted several hours, one of the largest flares observed by Yohkoh. We use here the data taken in flare mode around 03:06 UT, close to the flare maximum. While we present here just one of these flares, an extensive study of flares with this method will be the subject of future work (Reale et al. 1999).

Table 1 summarizes the Yohkoh/SXT observations used for our work, and their characteristics.

3.2. The Emission Measure during different phases of the solar cycle

Our work shows that the distribution of emission measure vs. temperature in the corona can vary by large factors, depending on the physical conditions of the corona. In Fig. 3a we show the EM during the three different phases of the solar cycle mentioned above, and in Fig. 3b the EM of the LDE of 2 November 92, close to its maximum luminosity, combined with the EM of the Sun on 6 Jan 92 (one example of the Sun close to the maximum of the cycle).

The emission measure shows the same general trend vs. temperature in all the three phases of the cycle: it first monotonically increases (up to 10^6 K), reaches a maximum between 1 and 2×10^6 K (the exact value however depends on the phase of activity), and then decreases monotonically towards higher temperatures.

From the maximum to the minimum of solar activity, the temperature of maximum emission measure shifts from $\approx 2 \times 10^6$ K to $\approx 1 \times 10^6$ K, and during the intermediate phase it is at 1.5×10^6 K.

From the maximum to the minimum of the solar cycle the EM decreases by orders of magnitude: by more than two orders of magnitude at any temperature above $\approx 3 \times 10^6$ K, and the slope of the EM distribution gets steeper during the minimum of the cycle. Also the emission measure below 10^6 K decreases during the minimum.

Outside flares, the characteristics of the emission measure at temperatures much higher than 10^7 K are not well defined since the flux ratio for standard filters used for full–disk observations (namely the Al.1, and the AlMg filters) is constant for temperatures above 10^7 K: quite likely there is some emission measure, but Yohkoh/SXT cannot determine its temperature precisely with this couple of filters.

In Fig. 3b, instead, the emission measure at and above 10^7 K comes mostly from the data taken in flare mode, i.e. with the filters Be119 and Al12, appropriate to sample temperatures around 10^7 K; the plasma characteristics up to a few 10^7 K are determined very accurately. A flare, as shown in Fig. 3b, adds a large, well separated, and transient distribution of EM at higher temperatures, typically around 10^7 K.

3.3. Rosat/PSPC-like spectra of the Sun

The first set of simulations folded the solar spectra through the Rosat/PSPC instrument response, as shown in Fig. 4. The Rosat/PSPC spectra were synthesized according to Eq. (2) from the EM distributions of Yohkoh/SXT observations of the maximum and of the minimum of the solar cycle (as of Fig. 3); we assume that the Rosat/PSPC observing time is 500 s for the Sun at the maximum and 5000 s for the Sun at the minimum. We assume that the Sun is at a distance of 1 pc in all our simulations for ease of conversion to the flux detected in stellar observations; the distance implies an easily detectable flux, even when the Sun is at the mininum of the cycle. Under these hypotheses such a twin of the Sun would yield in the focal plane of Rosat/PSPC ≈ 9.5 photons/s during maximum and ≈ 0.66 photons/s during the minimum. The exposure times have been selected so as to collect a total count of photons (respectively ≈ 4800 and ≈ 3300 photons) adequate to a spectral analysis with Rosat/PSPC and comparable to the values typically achieved when observing with this instrument.

Fig. 5 shows the analogous results for the flaring Sun. This spectrum clearly shows the presence of a hot component due to the flare. The solar flare here taken is a very intense one and, therefore, it could be easy to find solar flares in which the fitted hotter component is equivalent to (or smaller than) that of some flaring stars.

We now apply the Rosat standard analysis to the simulated stellar–like observation of the solar corona. We fit the Rosat spectra with multi–temperature model spectra excluding the channels with signal below the instrument's sensitivity and, if it occurs, omitting the tail of empty energy channels at the high energy part of the spectrum for an appropriate evaluation of the χ^2 (Ciaravella et al. 1997). We use the environment XSPEC V. 9.01 (Arnaud, 1996) for all the spectral analysis.

Fitting the synthesized observation of the maximum of the cycle in terms of one- or two-components of isothermal plasma, yields conditions typical of a moderately active star (Schmitt et al. 1990, Guedel et al 1998). The spectrum is poorly fitted with a single isothermal component: we get a $\overline{\chi}^2_r$, namely the reduced χ^2, of 4.3 with 21 degrees of freedom (d.o.f.) with a probability below 10^{-8} for the active Sun. The spectrum is well fitted, instead, with two different isothermal components, as it occurs for most stars (see Table 2); the temperatures of the two components are $\approx 1.1 \times 10^6$ K and $\approx 2.6 \times 10^6$ K [4]; the relevant fitted emission measures are 11.2×10^{49} cm^{-3} and 8.4×10^{49} cm^{-3}; for each fitting we show the value of $\overline{\chi}^2_r$. The total luminosity due to these two components is, approximately, 4.4×10^{27} erg s^{-1} in the Rosat/PSPC band ($0.1 - 3$ keV). This value is not necessarily the maximum X–ray luminosity of the solar corona, since we have not looked for it systematically.

Table 2 also shows the X-ray luminosity of the Sun near the peak of its cycle of activity, in the Rosat/PSPC band as derived integrating the emission from the SXT-derived EM(T) distribution (4.7×10^{27} erg s^{-1}), and the total luminosity, over the band from 0.01 to 100 keV, computed both from the fitting model and from the EM(T) distribution.

During the minimum of the solar cycle (June, 1 1994), the solar corona is approximately 20 times less luminous in the Rosat/PSPC band than at maximum (excluding flares). The decrease in the whole 0.01 – 100 keV band is, instead, close to a factor 10 because most of the emission of the solar corona at the minimum of the cycle occurs at lower photon energies. The spectral fitting of the solar corona at minimum is achieved with one temperature of 10^6 K and with an emission measure of $\approx 1.3 \times 10^{49}$ cm^{-3}. The total luminosity in the Rosat band is 2.3×10^{26} erg/s (2.7×10^{26} erg/s, instead, computed from the EM(T) distribution). The latter figures are typical of coronae of less active late–type stars observed with Rosat/PSPC (Micela, Pye and Sciortino, 1987) and Einstein/IPC (Schmitt et al., 1985).

The spectrum of the solar corona during the flare is poorly fitted by a single temperature component, yielding a $\overline{\chi}^2_r$ of 27.55 with 30 d.o.f.. The successfull fitting with two temperature yields a hot thermal component at a temperature typical of flaring plasma, much hotter than that of the non-flaring corona at cycle maximum. The emission measure of this hot component is one order of magnitude larger than the hot component of the non-flaring corona at cycle maximum. The temperature and emission measure values derived with the fitting are in Fig. 3, in order to compare them with the original EM(T) distribution. The fitted values reflect the maxima of the

---

[4]The hottest component for very active stars is around 10^7 K or more.

EM(T) distribution, and are above the original distribution they have to yield the same photon count.

In order to illustrate better the results of the spectral fitting in Fig. 6 we show, for the Sun at the maximum and at the minimum of the cycle and during the flare, the spectra at the telescope entrance computed for each of the fitted components and the analogous spectra synthesized from the EM(T).

3.4. ASCA/SIS-like spectra of the Sun and comparison with Rosat/PSPC

The same methods used to simulate Rosat observations were used to simulate ASCA observations of the Sun. Fig. 7 shows the synthesized X-ray spectra, as collected by ASCA/SIS, for the Sun at the maximum of the cycle and at the minimum. We have assumed a distance of 1 pc, as before, and an observing time of 5×10^4 s and 2×10^5 s, respectively, obtaining ≈ 17600 photon counts, for the maximum, and ≈ 960 photon counts, for the minimum. Fig. 8 shows the analogous result for the flaring Sun, assuming the same distance and an exposure time of 5×10^3 s; we get ≈ 28800 photons. The results of the spectral fittings for the three cases are reported in Table 2. Also for ASCA/SIS we have rejected the bins outside the instrument sensitivity and the tail of empty bins at the high energy part of the instrument. We have used XSPEC V.9.01 also in this case (see the preceding section on Rosat).

While the ASCA/SIS spectrum of the solar corona at maximum is fitted with two components, that of the solar corona at minimum can be fitted with a single component; for the flaring Sun even a two-temperature fit is inadequate and three thermal components are required. It is worth noting that many observations of ASCA/SIS are dedicated to very active stars, and even when these stars are not flaring, more than two thermal components are usually needed to fit the relevant spectra, with results more similar to the flaring Sun than to the Sun at maximum of the cycle. Taking these results at face value one may be lead to consider the flaring Sun, more than the Sun at maximum, similar to very active late–type stars.

Analogously to what done above for Rosat/PSPC, Fig. 9 shows, for each case, the spectra at the telescope entrance of the fitted components along with the analogous spectrum synthesized from the EM(T) for the Sun during the maximum and the minimum of the cycle, and during the flare.

Albeit slightly beyond the scope of this paper, it may be worth comparing the relative characteristics of the two observatories with the help of the results of the synthesized observations and the relevant fitting with thermal components. The two observatories have different sensitivities, spectral resolution and spectral bands: Rosat/PSPC has a larger effective area but virtually only below 2 keV, while ASCA/SIS is sensitive to photons above 0.5 keV up to 10 keV[5]; therefore it is more sensitive than Rosat/PSPC to the hottest plasma in the range of the Yohkoh/SXT temperature sensitivity. The spectral resolving power of ASCA/SIS is more than ten times higher than that of Rosat/PSPC. Incidentally we note that ASCA/SIS higher spectral resolving power makes it easier to fit multiple thermal components to the data, thereby identifying hotter components to the spectra.

In order to illustrate better the relative performance of Rosat/PSPC, ASCA/SIS and Yohkoh/SXT we report the relevant effective areas in the various bands in Fig. 10.

The temperatures obtained by fitting ASCA/SIS spectra are consistently higher than those which fit the Rosat/PSPC spectra for the same emission measure distribution of the Sun. This finding can be motivated by the harder spectral band of ASCA/SIS ($0.5 - 10$ keV) which, therefore, tends to give more relative weight to the emission of the hotter plasma, and hence to measure higher temperatures. The fitted values are shown in Fig. 3, analogously to those obtained for Rosat/PSPC; considerations analogous to those made for Rosat/PSPC spectra apply to them.

4. Discussion

In summary, our method uses spatially resolved X-ray images of the Sun, collected by Yohkoh/SXT, to derive the relevant full–disk coronal EM(T) and to compute from EM(T) the spectrum over a wide X-ray spectral band with the appropriate resolution. We are able to fold the derived spectra with the available spectral response of non–solar X-ray observatories, such as Rosat and ASCA, thus synthesizing the relevant focal plane spectrum of the solar corona.

As for the limits of our method, one limitation comes from the fact that we obtain only a single temperature for each pixel, in the SXT images we are studying. It is, therefore, in principle possible to miss information if there is a very wide distribution of temperatures along each pixel line–of–sight or, in any case, within it. Also it is worth noting that SXT tends to detect preferentially the hottest plasma within the pixel and within the instrument's sensitivity range (Brosius et al., 1997). One may then expect that the temperatures derived by SXT are the results of an averaging process which, within each pixel, is slightly biased toward higher temperatures.

Certainly, for our task of comparing the X-ray solar spectrum with those of other stars, it would be very convenient to have detailed X-ray spectral information directly from solar observations to begin with; since they are not available, we take advantage of X-ray observations of high angular resolution made over wide bands: the spectrum is obtained from the detailed EM(T) distributions that we generate from the broad–band solar images; the detailed spatial sampling, provided by Yohkoh/SXT images, simultaneously probes the relatively wide temperature range of the solar corona and acts as a substitute for the lacking spectral resolution.

[5]The first 18 channels of ASCA/SIS, i.e. all those below 0.5 keV, are typically discarded because affected by systematic errors.

Yohkoh/SXT is very sensitive to the relatively hot plasma in the corona (a characteristic which makes it an excellent tool to observe the plasma in flares and, more in general, in highly dynamic events); its sensitivity is lower for plasma around 10^6 K or below. However the contribution of this cooler plasma to EM(T) may be important to determine the spectrum detected by instruments very sensitive also at lower photon energies, such as Rosat/PSPC or XMM (the X-ray Multi-Mirror Mission).

In the light of the above considerations, a significant part of our effort has been devoted to devise a reliable method to handle the emission measure below 10^6 K, which, as described in more details in Paper I, can be severely affected by errors if one does not pay proper care. On the basis of extensive simulations, of a comparison of our results with those of EUV observations, and of having compared a few alternative methods of analysis, we are now confident of the reliability of the results on the EM that we derive with the filters used for the standard observations outside flares, even below 10^6 K. The same filters do not allow to derive a precise value of temperature for $T > 10^7$ K (Tsuneta et al. 1991). On one hand, outside flares, the amount of EM present in the solar corona at 10^7 K or higher is so low, in a relative sense, to have little influence on the overall solar spectrum as collected by the stellar instruments here considered; on the other hand, during flares, a different set of filters, very sensitive to flaring plasma, is used. As shown in Fig. 3b, flares contribute a very high amount of emission measure around and above 10^7 K. The total emission measure of a flare in the corona is comparable to that normally present around 2×10^6 K, and quite likely even larger in the largest flares. Therefore we are confident that whenever a significant amount of emission measure above 10^7 K is present, Yohkoh detects it.

Active regions normally dominate the intermediate-temperature domain of the EM(T) for a given image, in the range 2-5 $\times 10^6$ K (Orlando et al 1999b). Because of the non-linear response of the SXT filter ratio to temperature, the background coronal contributions to the distribution will tend to be obscured and not represented properly. However the active regions represent only small fractions of the total number of pixels, so an area-based correction for the missing low-temperature contributions would be small from any general background coronal material overlying the active region.

Our fitting of the Rosat/PSPC-like data in non-flaring moments yields significant components only at a few 10^6 K reflecting the fall of EM(T) at higher temperatures. The fittings made on active star's Rosat/PSPC spectra, instead, often yield a component around a few 10^6 K and another one around a few 10^7 K, the latter with an emission measure comparable, or even much larger, than that at 10^6 K.

The presence of a large amount of the emission measure at temperatures of 10^7 K or larger (Schmitt et al. 1990) in very active stellar coronae, even in absence of evident flares, has brought to the hypothesis of several flares occurring on the star with light curves overlapping to yield an apparently constant, hot and bright coronal component (cf. Guedel, 1997 and references therein).

It is to be noted that Rosat/PSPC observations of stars are usually fitted with two thermal components and that the two temperatures are often taken as evidence of a bi-modal temperature distribution in the corona with two dominating components at different temperatures. On the other hand, while our study of the solar corona at solar maximum is based on a smooth EM(T) with a single maximum, still the fitting of the synthesized Rosat/PSPC spectrum yields, with a good reduced $\overline{\chi}_r^2$ value, two thermal components. To some extent they indicate the temperature at which most of the emission measure is, but no bimodality exists in the original temperature distribution. Perhaps, on the basis of our findings, caution should be applied when interpreting Rosat/PSPC data.

In Fig. 11 we show, for the synthesized observations of the Sun with Rosat, the surface X-ray flux, defined as the X-ray luminosity in the Rosat/PSPC band (${L_x}^a$ in Table 2) divided by the solar surface area, vs. the hardness ratio HR, defined as (Schmitt 1997)

$$\mathrm{HR} = \frac{H - S}{H + S} \tag{3}$$

where S are the total counts in the PSPC pulse height channels 11-41 $(0.13 - 0.40$ keV) and H are the total counts in the channels 52-201 [6] $(0.55 - 1.95$ keV). We show the results relevant to the four cases studied here: minimum, intermediate phase, maximum of the solar cycle and peak of the large LDE flare (during the maximum of the solar cycle). This figure should be compared with the analogous Fig. 7 in Schmitt (1997) which however spans a much wider range of flux; we also show the borders of the region covered by late–type stars in Schmitt's paper. The results of Fig. 11 when compared to the results of stellar coronal physics shows: that the range spanned by solar X-ray luminosity is wide with respect to that of individual stars but small as compared to that of all the late–type stars, that the cases here examined fall well in the scenario of less active stars, that the Sun is in the low-luminosity low-HR part of the stellar distribution, and that the solar maximum certainly reaches fluxes (or luminosity) values higher than usually assumed (see however Vaiana and Rosner, 1978, for a few estimates of coronal luminosity over the whole spectrum), as discussed below in more detail.

We now discuss two examples of how our results help us to put the Sun more correctly in the perspective of stellar coronal physics. Albeit we have not looked systematically for the maximum solar X-ray luminosity in the Rosat band, the luminosity on 6 Jan 92, close to the maximum of the cycle, is larger than 10^{27} erg/s. In this respect it is worth noting that Schmitt (1997), referring to solar–type stars and on the basis of common knowledge of solar corona, states that "the median of the observed X–ray luminosity distribution function at $\log L_X = 27.5$ lies actually somewhat above solar maximum emission levels". Our result $\log L_X = 27.7$ for the Sun near (and probably slightly below) the maximum of luminosity, instead shows that such a median is *certainly below* the solar maximum emission levels.

[6] These are the "unbinned" pulse height channels. In many studies Rosat/PSPC spectra are re-binned, instead, over 34 channels.

Another point worth noting in this context is that Schmitt (1997) reports Rosat's detection of very faint nearby late–type stars with a surface flux of $\approx 10^4$ erg s^{-1} cm^{-2}. Since this value is very close to that derived by Hara et al. (1994) for a solar coronal hole, Schmitt concludes that Rosat/PSPC has been able to detect nearby stars entirely covered by coronal holes. Hara et al. reports several values of emission measure per unit surface depending on different corrections to the data. We have computed the relevant flux at Sun's surface in the Rosat/PSPC band, for Hara et al.'s highest and lowest valueis of emission measure per unit surface ($10^{26.22}$ cm^{-5} for $T = 1.83$ K and $10^{25.54}$ cm^{-5} for $T = 2.78$ K), using the MEKAL spectrum for easy comparison with our results, and the relevant values are shown in Fig. 11. The values of solar flux during the solar minimum are slightly above that of a coronal hole derived from Hara et al. It is worth noting that some faint and diffuse emission is still visible on the Sun at minimum and large polar coronal holes in the relevant images appear definitely dark regions, at variance from quiet areas. The inference is that Rosat/PSPC may have detected very faint nearby stars in conditions similar to those of the Sun during minimum of the cycle rather than entirely covered by coronal holes.

Another aspect worth noting is that the large changes of EM bring to large changes of X-ray luminosity, as we have shown before. In fact, the Sun's emission measure distribution above 10^6 K changes dramatically during the solar cycle: the peak of the distribution decreases by an order of magnitude but the decrease is even stronger at the highest temperatures, i.e. the EM also gets steeper, or "cooler". Since we have not searched systematically the Yohkoh data base, more extreme values of luminosity may easily exist. Such large changes of luminosity due to the solar cycle are not observed on stars (Stern 1998). Albeit extensive optical observations have shown that some G – type stars may exhibit a solar–like cycle (Baliunas et al., 1995), no evidence of an X-ray stellar cycle has been observed yet.

In other respects, our first results fit well in the stellar scenario: during phases of high activity, such as during the solar maximum, the solar corona is more luminous and, as a whole, hotter. Analogously the more luminous a stellar corona, the hotter it is. Therefore the physical mechanisms underlying the coronal phenomenon appear to be the same. However luminous and hot stellar coronae have not been observed to become faint and cool over the years, as instead it is observed on the Sun. A question is now whether the Sun spans a wider activity range, during the cycle, than most solar–type stars, or rather the Sun is just showing us a behaviour common among stars and we have been unable to detect it on other stars.

In the light of the above considerations it becomes important to provide X-ray observations of stars repeatedly and over appropriate time scales, in order to look for coronal cycles in late–type stars and, on the other hand, to obtain a set of data wider than the episodic observations we have made so far of most solar–type stars.

Extending the analogy from the corona of the Sun, an intermediate age and moderately active star, to the coronae of very active and young stars will require caution and deep insight; however a key aspect of our project is to explore if and to what extent we may apply our knowledge of the solar corona to understand the stellar observations.

5. Summary, Conclusions and Future Prospects

The work presented here and in the companion Paper I has given us a reliable method to derive the emission measure distribution EM(T) of the whole solar corona, from the Yohkoh/SXT data, and, from EM(T), to synthesize the global solar X-ray emission as it would be detected by non-solar X-ray telescopes.

This method provides a template for stellar data interpretation with the advantage of using real data and making very few model assumptions. These results are important to compare solar and stellar activity, to look for counterparts of solar phenomena and structures on stars and, more in general, to identify several aspects of stellar coronal phenomena with their solar counterparts.

The initial results are quite encouraging: they show that the analysis of solar spectra in stellar format yields plausible results, but they also put the solar coronal observations quantitatively in the more general stellar context. We find that the EM(T) distribution of the whole corona outside flares peaks around a few 10^6 K and decreases at higher T; the peak of this distribution is at slightly higher temperatures during the maximum of the solar cycle but, what is more important, the whole EM(T) is drastically lower during the minimum of the cycle and gets steeper on both sides of the peak. During flares, instead, a big peak occurs in the EM(T) around 10^7 K the exact value depending on the specific flare and on the phase of the flare. We find that during the solar cycle the Sun's luminosity in Rosat/PSPC band varies by a factor 20, a large long–term variation hardly detected on active stars and that the total luminosity computed from the best fitting thermal components is only 20% lower than that derived from the whole EM(T).

The synthesis of stellar-like spectra collected by non–solar X-ray observatories and the relevant spectral fittings are in line with the scenario of the Sun as a moderately active star. We have also compared our results of the Sun as an X-ray star with those about late–type stars by Schmitt (1997), showing that the Sun's cyclic variability covers a part of the lower range covered by the late–type stars of that paper and that the intrinsically faintest late–type stars that Rosat has detected may be equivalent to the Sun at the minimum of the cycle rather than to a Sun entirely covered by coronal holes.

We plan to tap in the future work the very large amount of information and of global conditions of the solar corona collected with Yohkoh/SXT to be used as a benchmark to interpret stellar X-ray observations. The large data set of Yohkoh/SXT allows us to study the solar coronal evolution since late 1991 until now, showing a large range of different conditions, from the very active phases and very energetic flares to the very quiet moments of the solar minimum.

We plan several studies which include global studies of the solar corona, mostly using the insight coming from the EM(T), and to study the solar-stellar connection in coronal physics. Our projects include: to study how the various causes of variability, i.e. flares, rotational modulation, active region evolution and the solar cycle, influence the evolution of the EM(T) and the variations of the X-ray emission; a general study of the evolution of the EM(T) during flares and a direct comparison of solar and stellar coronal characteristics. It will be also important to identify the contribution of the different parts of the corona to the global emission discriminating, for instance, that of the active regions cores from that of the fainter and older regions and, more in general, from that of the rest of the corona.

In order to study better the EM(T) up to a few 10^7 K we could use the data taken by Yohkoh/BCS (the Bent Crystal Spectrometer on board Yohkoh) on the line complexes of He-like ions of S XV, Ca XIX and Fe XXV. However, at variance with Yohkoh/SXT data, Yohkoh/BCS data have no spatial resolution and, therefore, integrate over the whole Sun. Data from Yohkoh/HXT, the Hard X-ray Telescope on board Yohkoh, especially from the softest channel, could also provide spatially resolved information on the hottest component of the corona, albeit without full–disk coverage and only during the flare mode.

At the other extreme of the temperature range covered by our analysis, it could be worthwhile to use observation of the Sun made simultaneously with the Solar and Heliospheric Observatory (SOHO), to achieve an accurate calibration of the EM(T) at the lower range of temperatures to which Yohkoh/SXT is sensitive. Indeed the coronal instruments on board SOHO, namely the Extreme ultraviolet Imaging Telescope (EIT), the Solar Ultraviolet Measurements of Emitted Radiation (SUMER) and the Coronal Diagnostics Spectrometer (CDS), are quite sensitive to plasma at temperatures up to $\approx 10^6$ K. We also plan to show the spectra computed from the Yohkoh/SXT-derived EM(T) and folded through the spectral response of other solar coronal instruments.

We acknowledge useful criticisms and suggestions from S. Serio, S. Sciortino, G. Micela, A.Maggio, L. Acton, S. Tsuneta, T. Watanabe and the hospitality at the Japan's Institute of Space and Astronautical Science (Tokyo). We acknowledge the stimulus of an anonymous referee to improve our method. This work has been partially supported by Agenzia Spaziale Italiana and by the Italian Ministero dell'Universitá e della Ricerca Scientifica e Tecnologica.

References

Arnaud, K. A., 1996, Astronomical Data Analysis Software and Systems V, Jacobi, G., and Barnes, J. (ed.), p. 17, ASP Conference Series

Baliunas et al. 1995, ApJ, 438, 269

Bornmann, P.L., and Matheson, L., 1990, A&A, 231, 525

Bornmann, P.L., Speich, D., Hirman, J., Matheson, L., Grubb, R., Garcia, H., Viereck, R., 1996, Proc. SPIE Vol. 2812, p. 291, "GOES-8 and Beyond", Edward R. Washwell Ed.

Brosius, J.W., et al., 1993, ApJ, 411, 410

Brosius, J.W., Davila, J.M., Thomas, R.J., Monsignori–Fossi, B.C., 1996, ApJS, 106, 143

Brosius, J.W., Davila, J.M., Thomas, R.J., Saba, J.L.R., Hara, H., Monsignori–Fossi, B.C., 1997, ApJ, 477, 969

Ciaravella, A., Maggio, A., Peres, G., 1997, A&A 320, 945

Craig, I.J.D., Brown, J.C., 1976, A&A 49, 239

Guedel, M. 1997, ApJ, 480, L121

Guedel, M., Guinan, E.F., Skinner, S.L., 1998, in Cool stars, stellar systems, and the Sun - 10th Cambridge workshop, R.A. Donahue and J.A. Bookbinder (ed.), PASP conf. series, in press

Hanser, F.A., Sellers, F.B., 1996, Proc. SPIE Vol. 2812, p. 344, "GOES-8 and Beyond", Edward R. Washwell Ed.

Hara, H., Tsuneta, S., Lemen, J.R., Acton, L.W., McTiernan, J.M., 1992, PASJ 44, L135

Hara, H., Tsuneta, S., Acton, L.W., Bruner, M.E., Lemen, J.R., Ogawara, Y., 1994, PASJ 46, 493

Kaastra, J.S. 1992, An X-Ray Spectral Code for Optically Thin Plasmas (Internal SRON-Leiden Report, updated version 2.0)

Kano, R. 1994, Univ of Tokyo Masters Thesis

Kano, R., & Tsuneta, S. 1995, ApJ, 454, 934

Landi, E. and Landini, M., 1997, in "The Corona and Solar Wind near Minimum Activity", Proc. of the 5th SOHO Workshop, A. Wilson (ed.), ESA SP-404

Maggio, A., Reale, F., Peres, G., Ciaravella, A., 1994, Comp. Phys. Comm., 81, 105

Mewe, R., Kaastra, J.S., Liedahl, D.A. 1995, Legacy, 6, 16

Mewe, R., Gronenschild, E.H.B.M., and van den Oord, G.H.J. 1985, A&AS, 62, 197

Mewe, R., Lemen, J.R., and van den Oord, G.H.J. 1986, A&AS, 65, 511

Micela, G., Pye, J., Sciortino, S., 1997, A&A, 320, 865

Morrison, M. 1994, "Yohkoh Analysis Guide. Volume 1-3"

Ogawara, Y., et al. 1991, Solar Phys., 136, 1

Orlando, S., Lou, Y.-Q., Rosner, R., Peres, G., J. Geophys. Res., 1996, 101, 24443

Orlando, S., Lou, Y.-Q., Peres, G., Rosner, R., J. Geophys. Res., 1997, 102, 24139

Orlando, S., Peres, G., Reale, F., Rosner, R., Hudson, H., 1999b, Proc. of the Second "Three-Islands" Euroconference "Stellar Cluster and Associations: Convection, Rotation, and Dynamos", held in Palermo (Italy) May 25 - 28, 1999, in preparation

Orlando, S., Peres, G., Reale, F., 1999a, Paper I, this same issue.

Orlando, S., Peres, G., Reale, F., Rosner, R., Hudson, H., 1998b, Cool stars, stellar systems, and the Sun - 10th Cambridge workshop, R.A. Donahue and J.A. Bookbinder (ed.), PASP conf. series, in press

Peres, G., Orlando, S., Reale, F., Rosner, R., Hudson, H. 1997, in Observational Plasma Astrophysics: Five Years of Yohkoh and beyond: Proceedings of the Yohkoh 5th Anniversary Symposium, Watanabe, Kosugi and Sterling (ed.), Kluwer Academic Publishers

Pottasch, S.R., 1965, ApJ 137, 946

Press, W.H., Flannery, B.P., Teukolsky, S.A., Vetterling, W.T. 1986, "Numerical Recipes", (New York: Cambridge Univ. Press)

Pye, J.P., et al. 1978, A&A, 65, 123

Reale, F., Orlando, S., Peres, G., et al., (1999), in preparation

Rosner, R., Golub, L., & Vaiana, G.S. 1985, ARA&A, 23, 413

Schadee, A., De Jaeger, C., Svestka, Z. 1983, Solar Pys., 89, 287

Schmitt, J.H.M.M., Harnden, F. R., Rosner, R., Peres, G., Serio, S. 1985, ApJ, 288, 751,

Schmitt, J.H.M.M., 1997, A&A 318, 215

Schmelz, J.T., Saba, J.L.R. and Strong, K.T., 1997, SPD meeting #29, #01.39

Stern, R.A., 1999, "X-ray Magnetic Activity and Variability in Stellar Coronae: What are the Limits of the Standard Picture?", in 'Solar and Stellar Activity: SImilarities and Differences," A.S.P. Conference Series Vol. 158 (C.J. Butler and J.G. Doyle, ed.), pp. 47-56.

Tsuneta, S., et al. 1991, Solar Phys., 136, 37

Vaiana, G.S., Krieger, A.S., Timothy, A.F. 1973, Solar Phys, 32, 81

Vaiana, G.S., Rosner, R., 1978, Ann. Rev. Astron. Astrophys., 16, 393-428

Vaiana, G.S., Krieger, A.S., Petrasso, R., Silk, J.K., Timothy, A.F. 1974, Proc. SPIE, 44, 185

Watanabe, T., Hara, H., Shimizu, T., Hiei, E., Bentley, R.D., Lang, J., Phillips, K.J.H., Pike C.D., Fludra, A., Bromage, B.J.I., Mariska, J., 1995, Solar Phys. 157, 69

Withbroe, G.L., 1975, Solar Phys. 45, 301

Withbroe, G.L., & Noyes, R.W. 1977, ARA&A, 15, 36

Yoshida, T., Tsuneta, S., 1996, ApJ, 459, 342

Fig. 1.— This figure illustrates the various phases of our method: from the Yohkoh/SXT images taken with two different filters, we derive the temperature and the emission measure in the pixels of the images; we then sort the emission measure values and build a histogram of EM vs. T. From the histogram we synthesize the emitted spectrum, with the help of one of the available spectral codes. Folding the spectrum with the response of the instrument of interest, as well as applying the observational effects (photon noise, distance of the source, exposure time, etc.) we obtain a realistic simulation of the solar corona observed as if it was a nearby star. To the spectra we can apply the standard data analysis appropriate to the instrument of interest.

Fig. 2.— The images of the Sun that we have selected to apply and illustrate our method. They have been taken on 6 Jan 92, around 21:45 UT (top), on 27 Jul 93 at 11:28 UT (middle), and on 1 Jun 94 at 6:35 UT (bottom), all through the Al (1265 A) filter. They are examples of maximum, intermediate and minimum phases of the solar cycle, respectively.

Fig. 3.— Distributions of the emission measure vs. temperature derived with our method for the three very different phases of the solar cycles shown in Fig. 2. The thick solid curve pertains to the 6 Jan 92 observation (solar maximum), the thin solid one to the 27 Jul 93 one and the dashed one to the 1 Jun 94 observation (solar minimum). The curve in the lower panel contains the contribution of the corona during the solar maximum (thick solid in upper panel) and of the LDE flare of 2 Nov 92. The error bars in each bin on the distributions are derived from the propagation of the fractional errors on T and EM obtained with the Standard Yohkoh Analysis System modified to consider the MEKAL spectral code (see text). We also show the results of the spectral fitting of the synthesized spectra folded through the Rosat/PSPC and ASCA/SIS spectral response; squares: fitting of Rosat/PSPC spectra, diamonds: fitting of ASCA/SIS spectra, large symbols: Sun at maximum of the cycle, small symbols: Sun at minimum. See also Table 2.

Fig. 4.— Rosat/PSPC synthesized spectra of the Sun (points with crosses yielding the error bars) from the maximum (top) and the minimum (bottom) phases of the cycle together with the best–fit multi–temperature MEKAL spectrum (solid histogram). The y–axis of the bottom panel shows the contribution, with its sign, of each bin to the total χ. We assume that the Sun is at a distance of 1 pc and the observing live time is 500 s for the Sun at maximum and 5000 s for the Sun at minimum.

Fig. 5.— Simulated Rosat/PSPC spectrum of the active Sun of 6 Jan 1992 plus the LDE flare of 2 Nov 92 assuming a distance of 1 pc and an exposure live time of 500 s.

Fig. 6.— Spectra of the corona synthesized with the MEKAL code directly from the EM(T) distribution (solid thick line) and from each of the isothermal components (solid thin line and dashed line) derived with the spectral fitting of Rosat/PSPC spectra, as reported in Table 2. Top panel: Sun at maximum. Middle panel: Sun at minimum. Bottom panel: flaring Sun. Each spectral bin is 6.1 eV wide.

Fig. 7.— The same as Fig. 4 but for ASCA/SIS observations with exposure times of 5×10^4 s for

the Sun at Maximum (top) and 2×10^5 s for the Sun at minimum of the cycle (bottom).

Fig. 8.— The same as Fig. 5 as seen with ASCA/SIS with an exposure time of 5×10^3 s.

Fig. 9.— The same as Fig. 6 for ASCA/SIS.

Fig. 10.— Upper panel: the effective area of Yohkoh/SXT including the two filters used for standard full Sun observations (marked as Al.1 and AlMg) and the two filters more frequently used for flare mode observations (Al12 and Be119). Lower panel: effective areas of Rosat/PSPC and ASCA/SIS

Fig. 11.— Solar X-ray flux (erg s^{-1} cm^{-2}), i.e. the total X-ray luminosity in the Rosat/PSPC band (${L_x}^a$ in Table 2) divided by the stellar surface area, vs. hardness ratio in the Rosat/PSPC band. We show the four phases of the solar activity which we have studied; from left to right: minimum, intermediate phase and near maximum of the solar cycle, and maximum phase of the large LDE flare. This figure should be compared with the analogous Fig. 7 of Schmitt (1997) on G stars which however extends to much higher stellar fluxes. The two lines mark the upper and the lower borders of the region covered by G stars in Schmitt paper. The circles mark the range of values of X-ray flux of the Sun entirely covered by coronal holes computed from Hara et al.(1994.

Table 1. Yohkoh observations

Day	Time (UT)	Filter	Exposure Time (ms)	Comment
6 January '92	21:38:28	Al.1	79	Sun at Maximum of Cycle
"	21:40:36	AlMg	79	"
"	21:51:16	Al.1	2689	"
"	21:53:24	AlMg	2689	"
27 July '93	11:26:35	Al.1	2668	Intermediate Sun
"	11:28:43	AlMg	5338	"
"	11:30:51	AlMg	168	"
"	11:32:59	Al.1	78	"
1 June '94	07:33:42	AlMg	5338	Sun at Minimum of Cycle
"	07:31:28	Al.1	2668	"
2 Nov '92	03:06:14	Al12	1.4	Flare Data
"	03:06:12	Be119	2.9	"

Table 2. Analysis of stellar-like solar spectra

	Sun at Maximum		Sun at Minimum		Flaring Sun	
	Rosat/PSPC	ASCA/SIS	Rosat/PSPC	ASCA/SIS	Rosat/PSPC	ASCA/SIS
t_{exp} (sec)	5×10^2	5×10^4	5×10^3	2×10^5	5×10^2	5×10^3
Nr of phot.	4774	17551	3291	961	12513	28787
Nr of chan.	23	58	21	28	32	183
$\overline{\chi}_r^2$	0.61	0.89	1.01	0.78	1.31	0.63
T_1 (10^6 K)	1.05 ± 0.08	2.16 ± 0.02	0.97 ± 0.03	1.78 ± 0.05	1.71 ± 0.06	2.49 ± 0.10
T_2 (10^6 K)	2.57 ± 0.15	5.65 ± 0.19	-	-	14.1 ± 0.32	12.4 ± 0.46
T_3 (10^6 K)	-	-	-	-	-	18.5 ± 1.1
EM_1 ($10^{49} cm^{-3}$)	11.22 ± 1.01	9.35 ± 0.22	1.25 ± 0.06	0.28 ± 0.06	17.6 ± 0.7	9.70 ± 0.81
EM_2 ($10^{49} cm^{-3}$)	8.35 ± 1.46	1.18 ± 0.14	-	-	75.3 ± 3.1	34.1 ± 7.5
EM_3 ($10^{49} cm^{-3}$)	-	-	-	-	-	46.7 ± 7.6
L_x ($10^{27} erg/s$) [a]	4.41 ± 0.45	1.42 ± 0.05	0.23 ± 0.01	0.022 ± 0.005	19.5 ± 0.8	14.6 ± 0.2
L_x ($10^{27} erg/s$) [b]	4.68	1.49	0.27	0.023	19.7	14.9
L_x ($10^{27} erg/s$) [c]	23.3 ± 2.2	8.23 ± 2.61	2.17 ± 0.11	0.34 ± 0.07	42.4 ± 1.6	26.1 ± 2.9
L_x ($10^{27} erg/s$) [d]	26.7		2.76		47.0	

[a]X–ray luminosity *in the instrument's spectral band* ($0.1-3$ keV for Rosat/PSPC and $0.5-10$ keV for ASCA/SIS) derived from the fitted isothermal components.

[b]X–ray luminosity *in the instrument's spectral band* computed from the original EM(T).

[c]The same as ([a]) but *over the 0.01 – 100 keV band.*

[d]The same as ([b]) but *over the 0.01 – 100 keV band.*

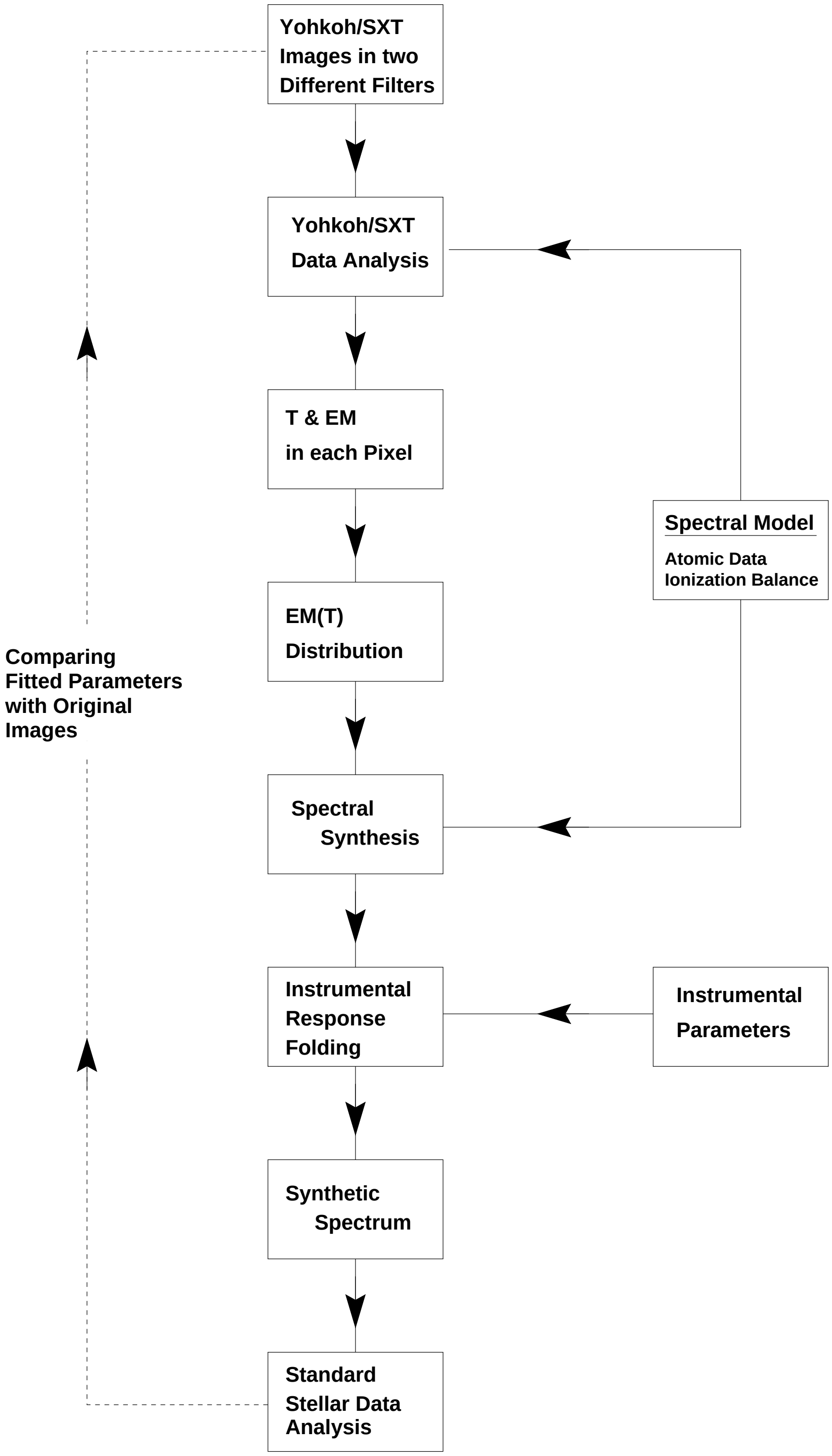
Yohkoh/SXT
Images in two
Different Filters
Yohkoh/SXT
Data Analysis
T & EM
in each Pixel
Spectral Model
Atomic Data
Ionization Balance
EM(T)
Distribution
Comparing
Fitted Parameters
with Original
Images
Spectral
Synthesis
Instrumental
Response
Folding
Instrumental
Parameters
Synthetic
Spectrum
Standard
Stellar Data
Analysis

Fig. 1.—

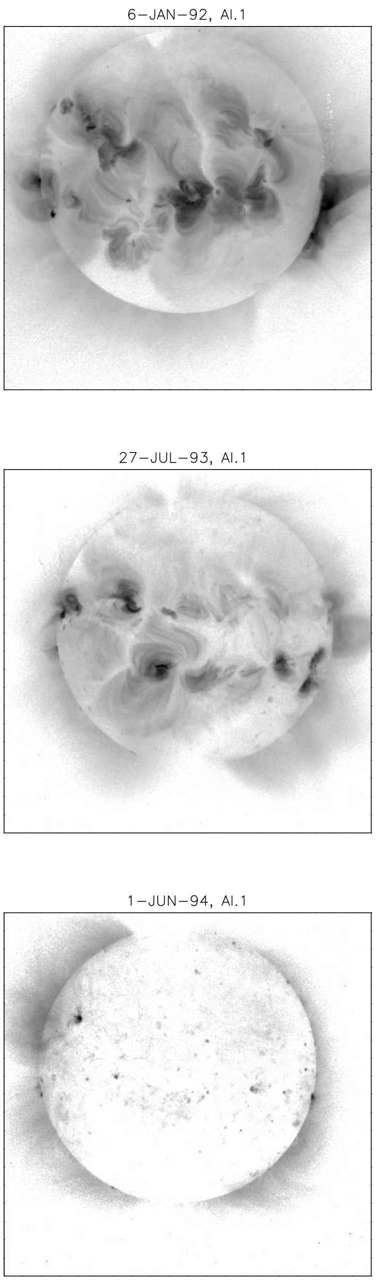

Fig. 2.—

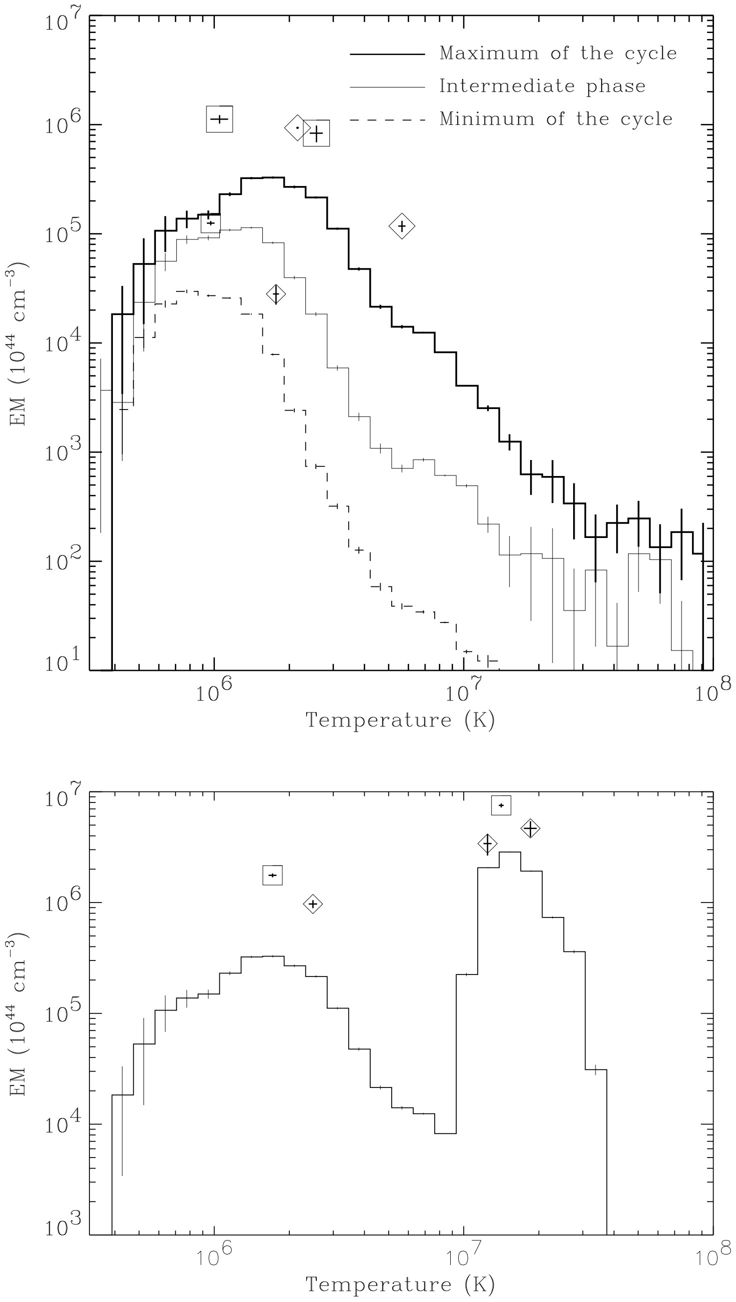
Maximum of the cycle
Intermediate phase
Minimum of the cycle
EM (10^{44} cm^{-3})
Temperature (K)
10^1
10^2
10^3
10^4
10^5
10^6
10^7
10^8

Fig. 3.—

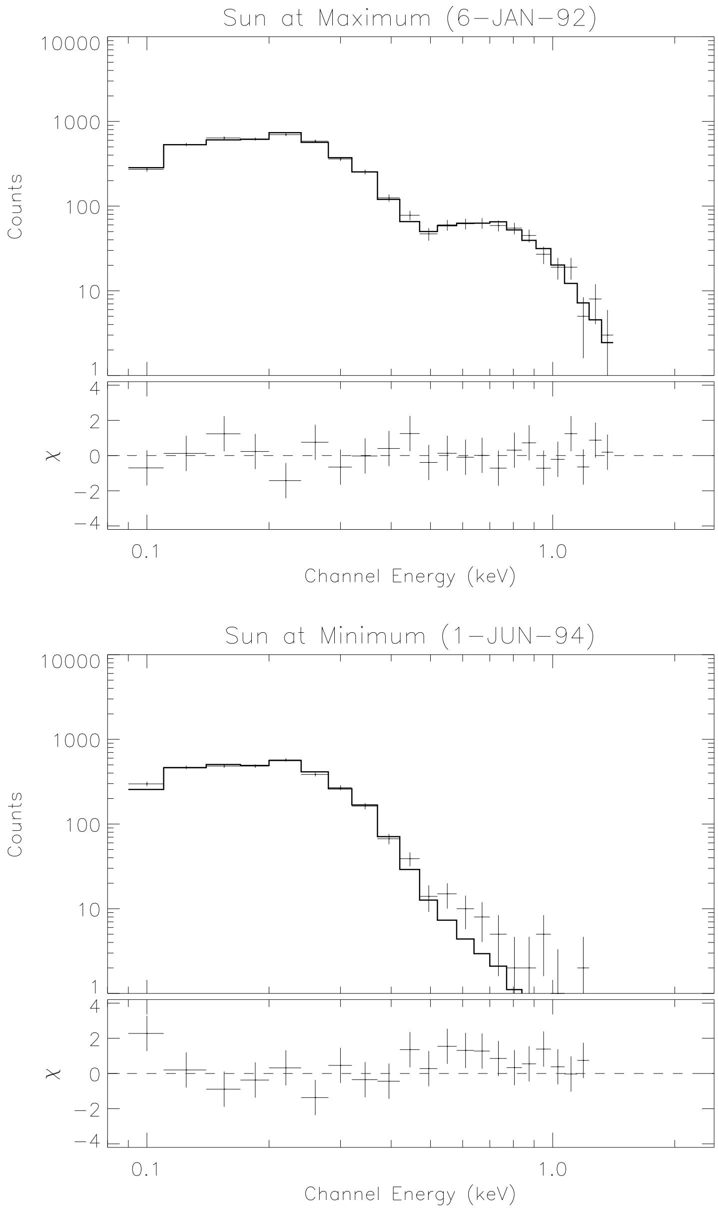
Sun at Maximum (6-JAN-92)
10000
1000
100
10
1
Counts
4
2
0
−2
−4
χ
0.1
1.0
Channel Energy (keV)
Sun at Minimum (1-JUN-94)
10000
1000
100
10
1
Counts
4
2
0
−2
−4
χ
0.1
1.0
Channel Energy (keV)

Fig. 4.—

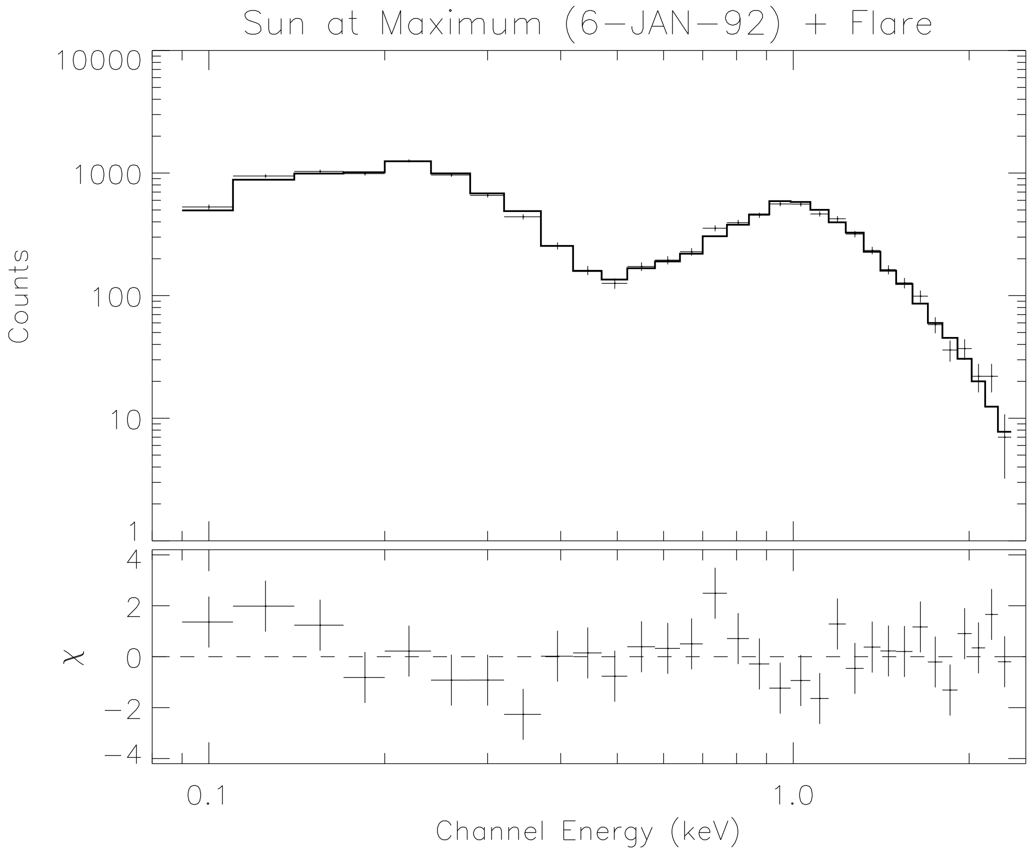
Sun at Maximum (6-JAN-92) + Flare
Counts
10000
1000
100
10
1
χ
4
2
0
−2
−4
0.1
1.0
Channel Energy (keV)

Fig. 5.—

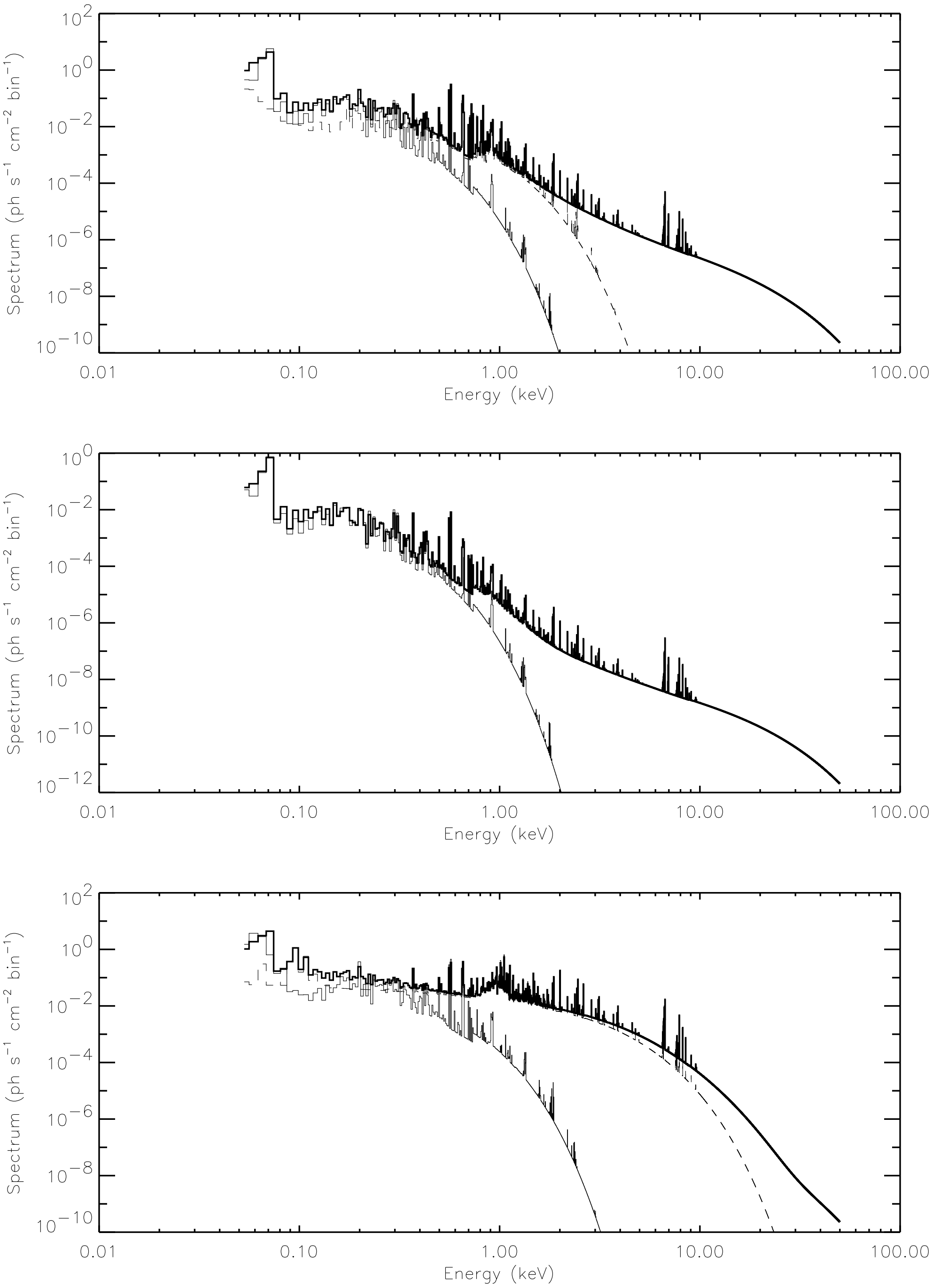
Spectrum (ph s^{-1} cm^{-2} bin^{-1})
10^{2}
10^{0}
10^{-2}
10^{-4}
10^{-6}
10^{-8}
10^{-10}
10^{-12}
0.01
0.10
1.00
10.00
100.00
Energy (keV)

Fig. 6.—

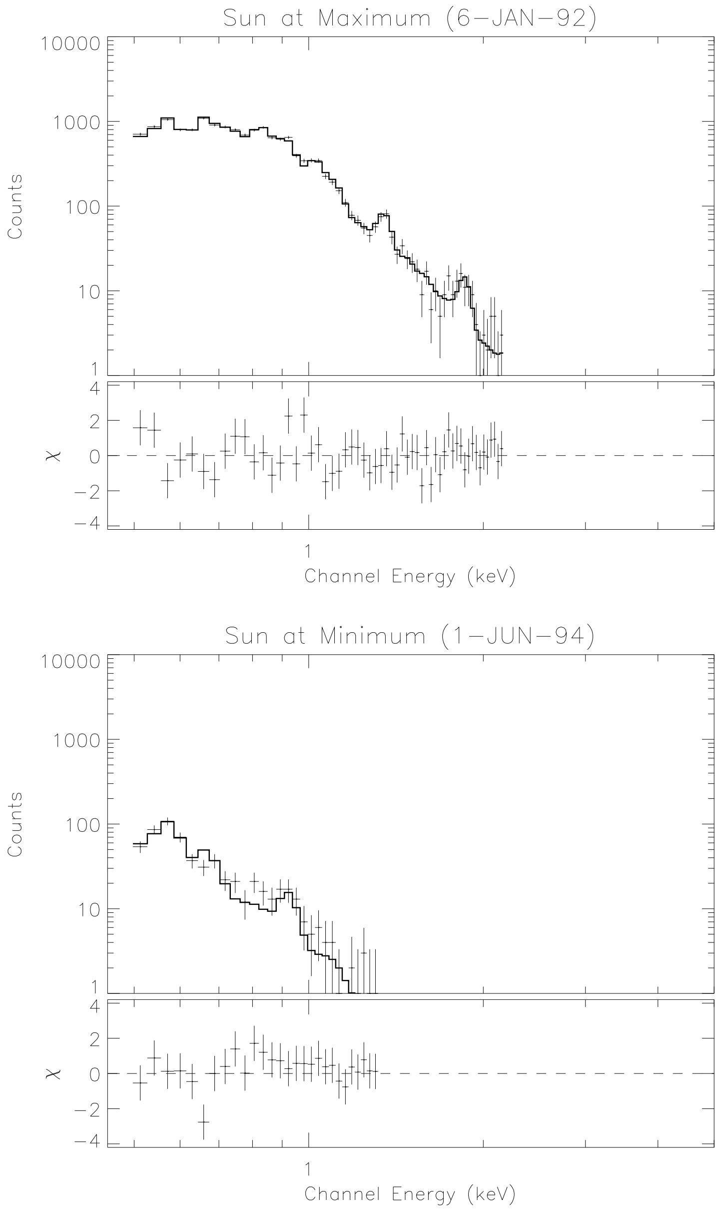

Sun at Maximum (6-JAN-92)
10000
1000
100
10
1
Counts
4
2
0
−2
−4
χ
1
Channel Energy (keV)
Sun at Minimum (1-JUN-94)
10000
1000
100
10
1
Counts
4
2
0
−2
−4
χ
1
Channel Energy (keV)

Fig. 7.—

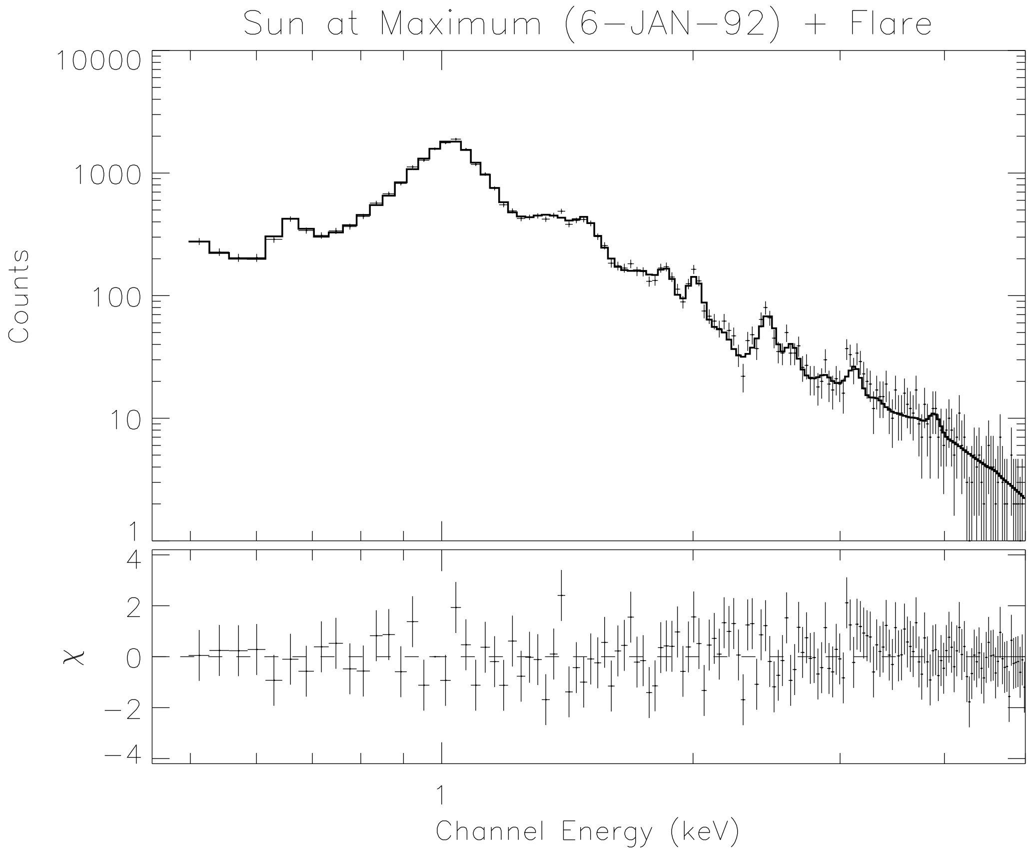
Sun at Maximum (6-JAN-92) + Flare
10000
1000
100
10
1
Counts
4
2
0
−2
−4
χ
1
Channel Energy (keV)

Fig. 8.—

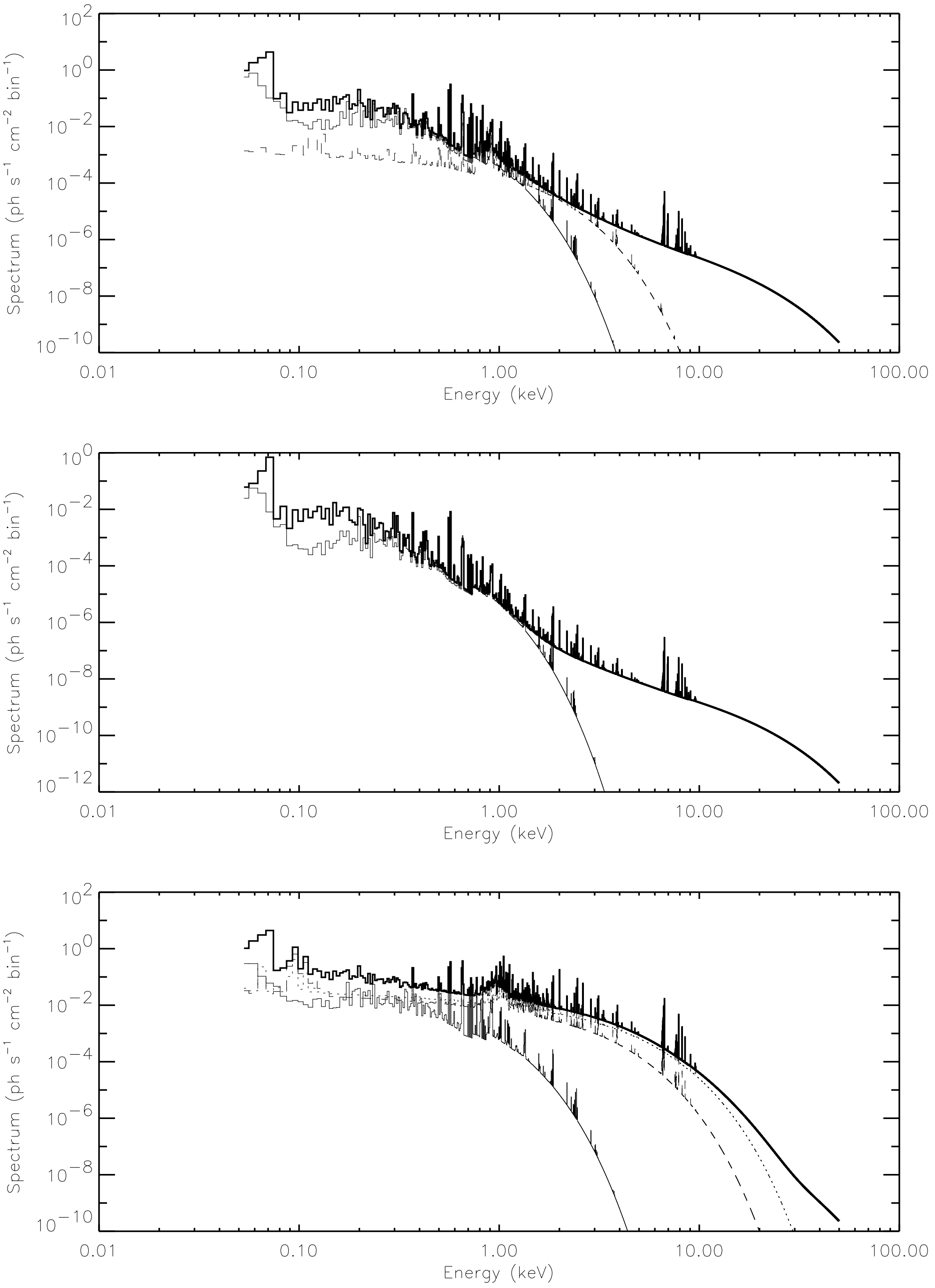
Spectrum (ph s^{-1} cm^{-2} bin^{-1})
Energy (keV)
0.01
0.10
1.00
10.00
100.00
Spectrum (ph s^{-1} cm^{-2} bin^{-1})
Energy (keV)
Spectrum (ph s^{-1} cm^{-2} bin^{-1})
Energy (keV)

Fig. 9.—

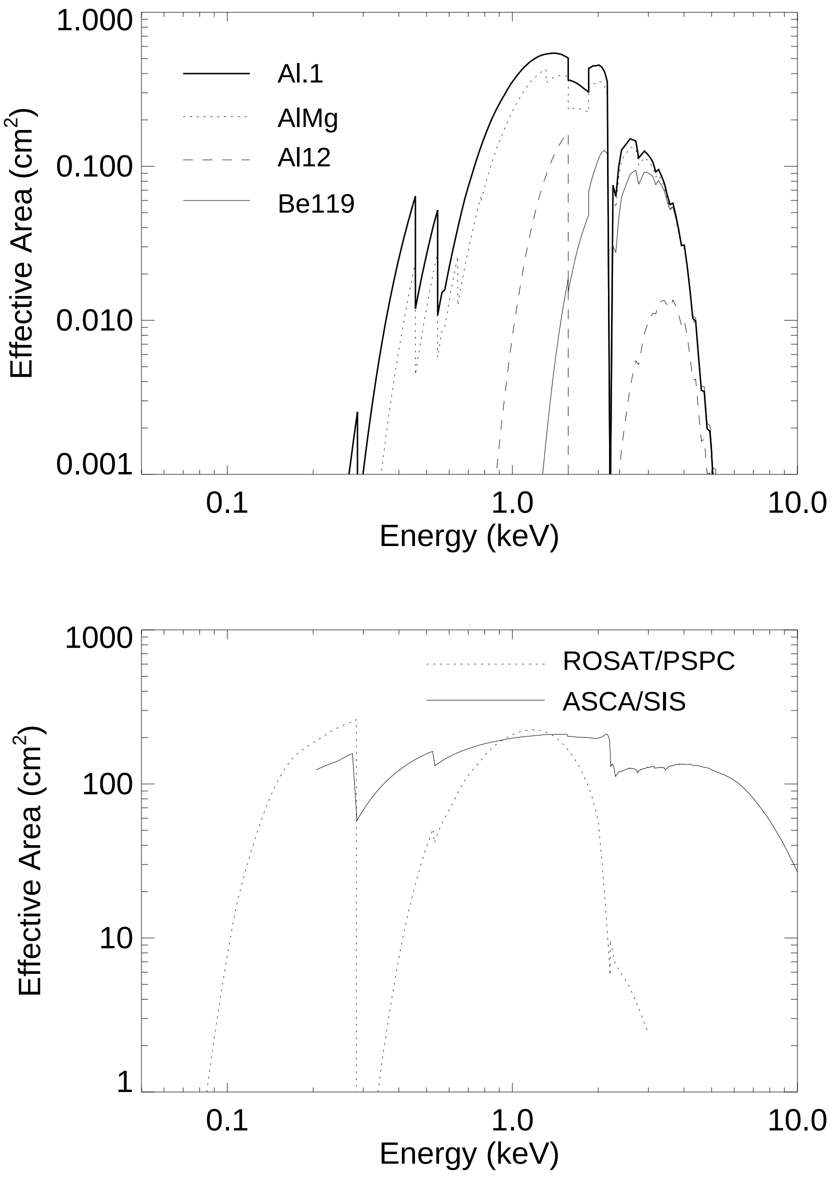

1.000
0.100
0.010
0.001
Effective Area (cm^2)
Al.1
AlMg
Al12
Be119
0.1
1.0
10.0
Energy (keV)
1000
100
10
1
Effective Area (cm^2)
ROSAT/PSPC
ASCA/SIS
0.1
1.0
10.0
Energy (keV)

Fig. 10.—

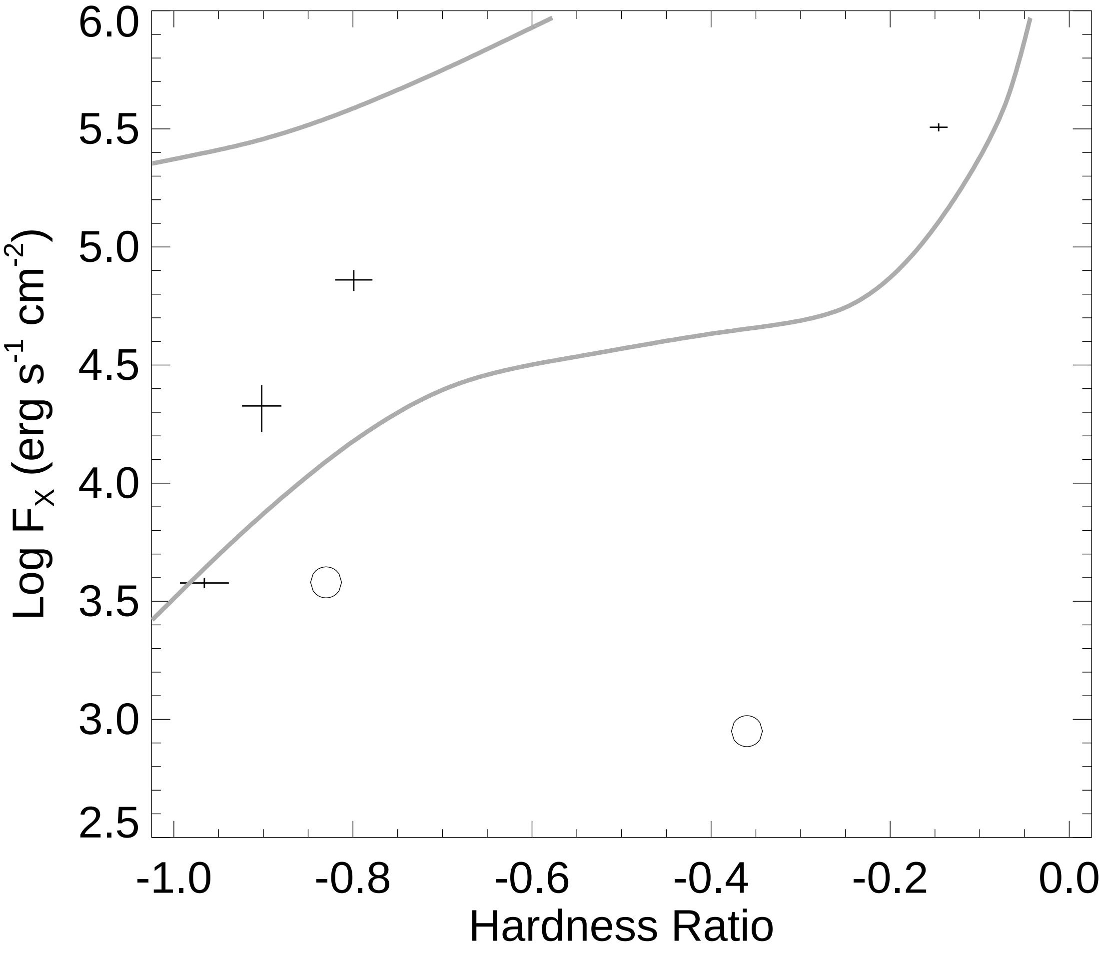

6.0
5.5
5.0
4.5
4.0
3.5
3.0
2.5
Log F$_X$ (erg s^{-1} cm^{-2})
-1.0
-0.8
-0.6
-0.4
-0.2
0.0
Hardness Ratio

Fig. 11.—